Rapid Communications

Cooperative orbital moments and edge magnetoresistance in monolayer WTe_2

Arpit Arora,[1] Li-kun Shi,[1] and Justin C. W. Song[1,2,*]

[1]*Division of Physics and Applied Physics, Nanyang Technological University, Singapore 637371*

[2]*Institute of High Performance Computing, Agency for Science, Technology, and Research, Singapore 138632*

(Received 16 June 2020; accepted 9 September 2020; published 5 October 2020)

We argue that edge electrons in monolayer WTe_2 can possess a "cooperative" orbital moment (COM) that critically impacts its edge magnetoresistance behavior. Arising from the cooperative action of both Rashba and Ising spin-orbit coupling, COM quickly achieves large magnitudes (of the order of a few Bohr magnetons) even for relatively small spin-orbit coupling strengths. As we explain, such large COM magnitudes arise from an unconventional cooperative spin canting of edge spins when Rashba and Ising spin-orbit coupling act together. Strikingly, COM can compete with spin moments to produce an unusual anisotropic edge magnetoresistance oriented at an oblique angle. In particular, this competition produces a direction along which **B** is ineffective at gapping out the edge spectrum, leaving it nearly gapless. As a result, large contrasts in gap sizes appear as **B** is rotated, granting a giant anisotropic magnetoresistance as large as several million percent at 10 T and low temperature.

DOI: 10.1103/PhysRevB.102.161402

Quantum spin Hall (QSH) insulators are highly sensitive to magnetic field. Protected by time-reversal symmetry, QSH insulators exhibit robust gapless edge states and edge electrons that do not backscatter [1–11]. This protection is readily lifted when a magnetic field **B** is applied to open a gap in the edge spectrum to produce large edge magnetoresistance [4,5,12] even at relatively low fields. When **B** is applied in plane, the edge gap is determined by spin moments. For out-of-plane **B**, however, the edge gap is controlled by the orbital structure of the edge states [5,12–14] with an induced edge gap depending sensitively on the strength of the topological band inversion M [5,12,13]. In systems with only a small topological band inversion $M \sim 10$ meV such as HgTe and InAs/GaSb quantum well QSH platforms [4,5,10,15–17], the out-of-plane magnetic-field-induced gap can be very large and is dominated by an orbital effect with giant effective (orbital) g factors of 40–50 [5,12,13].

In contrast, the QSH insulator monolayer WTe_2 [18–21], while possessing similar low dissipation transport that persists to high temperatures, possesses a large topological band inversion $2M = 1$ eV [11,19] dominating over other energy scales. As such, the ordinary orbital edge magnetoresponse is expected to be severely muted, suppressed by factors of several thousand in comparison with their small M counterparts [5,12,13]; this should dramatically quench the out-of-plane magnetoresponse. However, recent measurements report an unexpected sizable edge gap opening [18,20] in monolayer WTe_2 even when B is applied out of plane.

Here, we argue that an unusual *cooperative* effect yields a sizable edge orbital response in monolayer WTe_2 and a large out-of-plane magnetoresponse. In particular, we find that the combined action of Rashba spin-orbit coupling (SOC) working together with Ising SOC produces a cooperative orbital magnetic moment (COM). Crucially, COM achieves sizable values (of the order of a few Bohr magnetons) even when

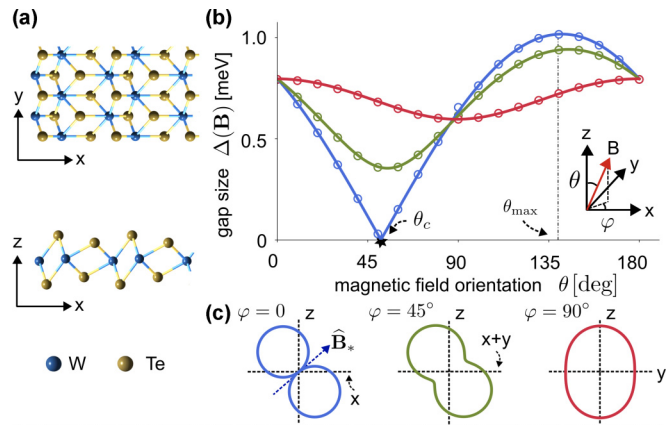

FIG. 1. (a) Crystal structure of monolayer WTe_2. (b) COM yields a significant out-of-plane magnetic-field-induced gap $\Delta(\mathbf{B} = B_z\hat{\mathbf{z}})$ ($\theta = 0^\circ$) in the edge state spectrum (for an x edge). Away from $\theta = 0^\circ$, $\Delta(\mathbf{B})$ displays an anisotropic angular dependence that depends on azimuthal φ and polar θ angles. Here, $\mathbf{B} = |\mathbf{B}|(\cos\varphi\sin\theta, \sin\varphi\sin\theta, \cos\theta)$, and blue, green, and red denote $\varphi = 0, 45^\circ, 90^\circ$ (see inset). When $\varphi = 0$ (blue), the gap nearly vanishes at $\theta_c = 51^\circ$ with a gap value at the starred point $\Delta(\mathbf{B}_*) = 3.5$ μeV. (c) Polar plot of $\Delta(\mathbf{B})$ shown for various planes at $\varphi = 0, 45^\circ, 90^\circ$ (blue, green, red). The starred point in (b) manifests in a direction $\widehat{\mathbf{B}}_*$ (blue dotted arrow) wherein the **B** field is ineffective at gapping the edge spectrum. In all plots, solid lines indicate a full gap from Eq. (1) with effective gyromagnetic coefficients (off diagonal in Fig. 2; for diagonal, see SM [24]). Circles are gaps obtained from the edge spectrum ENS. We have taken $\delta_x = 40$ meV, $\delta_z = 70$ meV, and $|\mathbf{B}| = 7$ T as an illustration.

*justinsong@ntu.edu.sg

large M far exceeds both Rashba and Ising SOC magnitudes. COM is sustained only when Rashba and Ising SOC coexist. For example, in the absence of Ising SOC, COM vanishes, and the orbital magnetic response is suppressed by two orders of magnitude. As we explain below, COM is particularly pronounced in WTe_2 due to its misaligned Te atoms in the top and bottom layers [see Fig. 1(a)] that inextricably link Rashba and Ising SOC [22,23].

COM yields a significant out-of-plane magnetic-field-induced gap $\Delta(\mathbf{B} = B_z\hat{\mathbf{z}})$ [Fig. 1(b)] consistent with recent measurements [18,20]. Interestingly, when $\mathbf{B}$ is rotated away from $\hat{\mathbf{z}}$, COM competes with spin moments to produce an anisotropic $\Delta(\mathbf{B})$ with minima canted at an angle oblique to either in-plane or out-of-plane directions [Figs. 1(b) and 1(c)]. Strikingly, the $\mathbf{B}$-field-induced gap almost vanishes at θ_c when $\mathbf{B}$ lies in the x-z plane. This defines a direction $\widehat{\mathbf{B}}_* = (\sin\theta_c, 0, \cos\theta_c)$ in three-dimensional space along which the magnetic field is ineffective at gapping the edge spectrum even for large magnitudes of $\mathbf{B}$. This produces a giant anisotropic edge magnetoresistance (AMR) as large as several million percent at low temperatures and $|\mathbf{B}| = 10$ T.

We begin with a symmetry analysis of the gap opening in the edge states under an applied magnetic field. For simplicity, we concentrate on QSH edge states along the x edge,

$$H^{\text{edge}}(k_x) = \tilde{v}\sigma_z k_x + \frac{\mu_B}{2}\sum_{ij} g_{ij}\sigma_i B_j, \tag{1}$$

where $\sigma_{x,y,z}$ are Pauli matrices that capture a mixed orbital and spin degree of freedom [see Eq. (5)], $\tilde{v}$ is the velocity of the edge state, $i, j = \{x, y, z\}$, and B_j is the magnetic field along the j direction. Here, g_{ij} are effective gyromagnetic coefficients, and μ_B is the Bohr magneton. Here, we have taken the lowest-symmetry-allowed terms in k and B.

Of particular interest are off-diagonal g_{xz} and g_{yz} that determine the gap opening when a z-oriented magnetic field is applied; we note that $g_{zz}\sigma_z B_z$ only shifts the edge spectrum, leaving it gapless. Symmetry constrains the allowable terms in Eq. (1). As an illustration, consider a mirror operation in $z \to -z : \mathcal{M}_z$ [see also Supplemental Material (SM) [24] and Ref. [25] therein]. As expected, $\mathcal{M}_z$ leaves the first term of Eq. (1) invariant. However, the second term transforms as $\mathcal{M}_z^{-1}[g_{ij}\sigma_i B_j]\mathcal{M}_z$. As a result, when the mirror in z is preserved, g_{xz} and g_{yz} terms vanish; they are allowed when $\mathcal{M}_z$ is broken. As we will see, these arise through Rashba and Ising SOC.

We now turn to a microscopic description of the edge states. First, we examine a 4×4 minimal model for the electronic bulk of monolayer WTe_2 [22,23] as $\mathcal{H} = \mathcal{H}_0 + \mathcal{H}_R + \mathcal{H}_I$. The Bernevig-Hughes-Zhang (BHZ) Hamiltonian $\mathcal{H}_0$ captures the essential topological features of the QSH phase,

$$\mathcal{H}_0(k_x, k_y) = m_{\mathbf{k}} s_0\tau_z + v_x k_x s_z\tau_x - v_y k_y s_0\tau_y, \tag{2}$$

where $s_{x,y,z}$ and $\tau_{x,y,z}$ are Pauli matrices for the spin and orbital degrees of freedom, respectively, and $s_0 = \mathbb{I}_{2\times 2}$. Here, $m_{\mathbf{k}} = M - C_x k_x^2 - C_y k_y^2$ with $M, C_x, C_y > 0$, $2M = 1$ eV captures the strong topological band inversion found in monolayer WTe_2, and $v_{x,y}/\hbar$ are the Dirac velocities along the x and y directions [see Fig. 1(a)].

Rashba $\mathcal{H}_R$ couple spin blocks and Ising $\mathcal{H}_I$ mix the orbital textures [22,23],

$$\mathcal{H}_R = -\delta_x s_x\tau_y, \quad \mathcal{H}_I = -\delta_z s_z\tau_y, \tag{3}$$

where $\delta_{z,x}$ describes the strength of Ising and Rashba spin-orbit coupling, respectively.

We note that $\mathcal{H}_{R,I}$ in monolayer WTe_2 can originate from a variety of sources that include, for example, an applied electric field [22,23], coupling with the substrate, edge electric fields, or even a buckling of monolayer WTe_2 into a T_d phase [22]; recently, inversion breaking in monolayer WTe_2 has been detected via photocurrent imaging [22]. Regardless of its origin, these mix the spin sectors on Eq. (2) and impact the edge magnetoresponse [5,12,13,26,27].

In order to construct the edge Hamiltonian from the topological band inversion encoded in Eq. (2), we examine an edge along the x direction [Fig. 1(a)], where monolayer WTe_2 electrons occupy $y \geqslant 0$; $y < 0$ is the vacuum. For each k_x, two topological edge states emerge with a gapless spectrum traversing the bulk band gap when $\mathbf{B} = \mathbf{0}$ [1,2,5,6,10,13]; these can be directly obtained by an exact numerical solution (ENS) of the coupled partial differential equation in $\mathcal{H}$ when $k_y \to -i\partial_y$ (see SM [24]).

To clearly exhibit the role $\mathcal{H}_{R,I}$ plays, however, we analyze the structure of the edge wave functions. In so doing, we write the edge zero modes $|\Psi_s\rangle$,

$$\langle \mathbf{r}|\Psi_s\rangle = \sum_n a_n^s \exp\left(-y/\lambda_n^s\right)|u_n^s\rangle, \tag{4}$$

where $s = \pm 1$, λ_n^s are decay lengths of the edge state into the bulk, and $|u_n^s\rangle$ are pseudospins capturing the relative spin and orbital composition of the zero modes; these are obtained from solving $[\mathcal{H}(0, i\lambda_n^s)]|u_n^s\rangle = 0$. Here, the index $n = \pm 1$ arises from quadratic $m_{\mathbf{k}}$, and $a_{+1}^s = -a_{-1}^s$ are normalization constants that ensure the wave function vanishes at $y = 0$ as well as far from the edge $\Psi(y = 0) = \Psi(y \to \infty) = 0$.

Using the edge zero modes in Eq. (4) we directly construct the edge Hamiltonian by projecting the bulk Hamiltonian $\mathcal{H}_0(k_x, 0)$ onto the zero modes along the edge [Eq. (4)]. We find the eigenstates of the edge Hamiltonian $\{|\Phi_1\rangle, |\Phi_2\rangle\}$ are

$$\begin{pmatrix}|\Phi_1\rangle\\ |\Phi_2\rangle\end{pmatrix} = \begin{pmatrix}\cos\frac{\chi_1}{2}e^{-i\chi_2/2} & \sin\frac{\chi_1}{2}e^{i\chi_2/2}\\ \sin\frac{\chi_1}{2}e^{-i\chi_2/2} & -\cos\frac{\chi_1}{2}e^{i\chi_2/2}\end{pmatrix}\begin{pmatrix}|\Psi_+\rangle\\ |\Psi_-\rangle\end{pmatrix}. \tag{5}$$

In this basis, $\{|\Phi_1\rangle, |\Phi_2\rangle\}$, the edge Hamiltonian is diagonal and can be written as the first term of Eq. (1). Keeping only leading-order terms in $1/M$ (see SM [24]), we have $\tan\chi_1 \approx \text{sgn}(\delta_x)|\Gamma|/\gamma$ and $\tan\chi_2 \approx \text{Im}[\Gamma]/\text{Re}[\Gamma]$, where $\text{Re}[\Gamma] \approx \delta_x[1/(\delta) - \delta C_y/(v_y^2 M)]$ and $\text{Im}[\Gamma] \approx \delta_x[(v_y^2 M - \delta^2 C_y)/(4M^3 C_y)]$ is controlled by Rashba SOC, and $\gamma \approx \delta_z/\delta$ is controlled by Ising coupling SOC. The zero modes $|\Psi_\pm\rangle$ on the right-hand side of Eq. (5) possess pseudospinors that read (to leading order) as

$$|u_n^s\rangle = \mathcal{N}_s(\Sigma_s, \Sigma_s, 1, 1)^T, \quad \Sigma_s = (\delta_z + s\delta)/\delta_x, \tag{6}$$

where $\mathcal{N}_+ = [2(\Sigma_+^2 + 1)]^{-1/2}$ and $\mathcal{N}_- = \text{sgn}(\delta_x)[2(\Sigma_-^2 + 1)]^{-1/2}$ and $\delta = \sqrt{\delta_x^2 + \delta_z^2}$ with

$$\left[\lambda_n^s\right]^{-1} = \frac{v_y}{2C_y} + \frac{n\delta}{2\sqrt{MC_y}} - ins\sqrt{\frac{M}{C_y}} + \sqrt{\frac{M}{C_y}}\mathcal{O}(\eta^2), \tag{7}$$

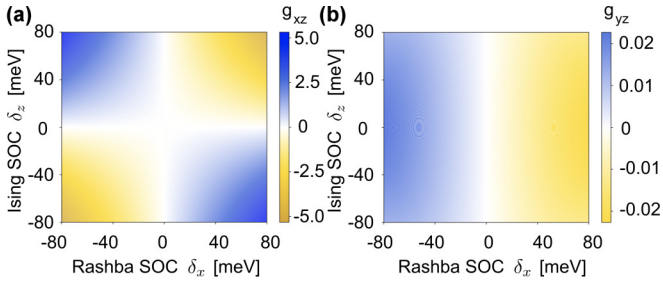

FIG. 2. Effective gyromagnetic coefficients for a perpendicular magnetic field for the edge parallel to the mirror axis (x axis) obtained from a numerical evaluation of edge eigenstates in Eq. (5) (see text). (a) shows the gyromagnetic coefficient corresponding to COM, g_{xz}, which arises from the combined action of finite Rashba and Ising SOC, and (b) displays g_{yz}, the gyromagnetic coefficient that corresponds to an ordinary orbital response [5,12,13]. The latter only requires a nonzero Rashba SOC. Strikingly, g_{xz} [(a)] is two orders of magnitude larger than g_{yz} [(b)]. Here, we have used the same WTe_2 parameters as Fig. 1.

where dimensionless $\eta = v_y/(2\sqrt{MC})$ is small due to the strong topological band inversion in monolayer WTe_2. Using typical parameters for monolayer WTe_2 we find $\eta = 0.15$ is small. At $\mathbf{B} = \mathbf{0}$, $\{|\Phi_1\rangle, |\Phi_2\rangle\}$ in Eq. (5) compose the gapless QSH edge states that propagate with renormalized edge velocity $\tilde{v} = v_x\sqrt{\gamma^2 + |\Gamma|^2}$ [see Eq. (1)].

The spin orientation of the edge states is directly controlled by δ_x, δ_z. For example, when $\delta_z, \delta_x = 0$, $\{|\Phi_1\rangle, |\Phi_2\rangle\}$ in Eq. (5) are eigenstates of s_z: $\{(1,1,0,0)^T, (0,0,1,1)^T\}$. When $\delta_z, \delta_x \neq 0$, however, $\{|\Phi_1\rangle, |\Phi_2\rangle\}$ can in general cant away from the poles of a Bloch sphere (where north/south correspond to spin up/down). Such a rotation of edge spin orientations is readily found in the familiar HgTe QSH systems, where small δ_x leads to significant canting of spins on the edge since $M \sim$ several meV is small in those systems [13]. In contrast, large $2M = 1$ eV in WTe_2 suppresses the power of $\mathcal{H}_R$ or $\mathcal{H}_I$ *individually* in canting the edge spin orientation. Indeed, when $\delta_z = 0$ (so that $\chi_1 = 90^\circ$) and $\delta_x \neq 0$ the spin orientations barely cant away from the north/south pole since $\chi_2 \approx 2(\delta_x/M)\eta^2 \sim 0.005$ rad $= 0.3^\circ$ using $\delta_x \approx 50$ meV. Similarly, for $\delta_z \neq 0$ but $\delta_x = 0$, the edge spins continue to be aligned along s_z.

Instead, when *both* $\delta_x, \delta_z \neq 0$ a cooperative effect ensues to produce a large spin canting which is relatively insensitive to M. For typical values of δ_x, δ_z in WTe_2 we find $|\tan\chi_1| \sim$ unity signaling significant rotation away from $\mathbf{s}_z$. As we now discuss, this departure (in how the WTe_2 edge spin orientation behaves) from the more familiar case of HgTe/CdTe leads to COM and a distinctly different edge magnetoresponse.

We first concentrate on the edge orbital magnetoresponse which is particularly sensitive to spin orientation. Orbital motion can be described via minimal coupling in the bulk as $\mathcal{H}_0(-eyB_z/\hbar c, 0)$, where we have used a Landau gauge. Using the $\{|\Phi_1\rangle, |\Phi_2\rangle\}$ basis, we analyze the effect of the orbital motion on the edge electrons via $\langle\Phi_1|\mathcal{H}_0(-eyB_z/\hbar c, 0)|\Phi_2\rangle$. This produces B_z induced terms in Eq. (1) that gap the edge spectrum, namely g_{xz} and g_{yz}; these terms do not commute with σ_z. g_{xz} and g_{yz} are shown in Figs. 2(a) and 2(b) obtained by computing the above matrix element with a numerical solution of Eq. (5) keeping all orders.

Strikingly, Figs. 2(a) and 2(b) reveal that g_{xz} is more than a 100 times larger than g_{yz}. Further, while g_{yz} is finite so long as $\delta_x \neq 0$, g_{xz} arises only when *both* $\delta_x, \delta_z \neq 0$. The dichotomy in magnitudes and behavior of g_{xz} and g_{yz} vividly displays a *cooperative* effect: In the presence of both Ising and Rashba SOC, large orbital gaps can be opened by B_z (from g_{xz}); in contrast, the orbital response is severely suppressed when $\delta_x \neq 0, \delta_z = 0$ (from g_{yz}).

We identify the $\delta_x, \delta_z \neq 0$ cooperative behavior of g_{xz} as COM. Importantly, sizable COM persists even as M overwhelms δ_x, δ_z. This large COM value directly proceeds from the strong canting of spins in the edge eigenstates when both $\delta_x, \delta_z \neq 0$, as discussed above. To see this link explicitly, we analyze the M dependence of g_{xz} directly, keeping only the leading-order terms in Eq. (5),

$$g_{xz} \approx -\frac{A\delta_x\delta_z}{M} = -1.62\frac{(\delta_x[\text{meV}]/50)(\delta_z[\text{meV}]/50)}{(M[\text{meV}]/500)}, \quad (8)$$

where $A = 8m_e v_x C_y^2/(\hbar^2 v_y^3)$ with m_e the free-electron mass, and in the second line we have used typical ranges of fitted values for WTe_2 band parameters (see SM [24]). Comparing g_{xz} in Fig. 2(a) and Eq. (1), we find the strong canting of spins enables a COM magnitude of several Bohr magnetons for WTe_2. In contrast, $g_{yz} \sim 0.02$ [Fig. 2(b)] is highly suppressed, and scales as δ_x/M^2 mirroring the small χ_2 canting in the edge spins (suppressed by large M) in much the same fashion as that found for the edge orbital moments of HgTe [5,13].

While the cooperative spin canting mechanism and COM are general effects, we expect COM to be especially pronounced in monolayer WTe_2 due to its misaligned Te atoms in the top and bottom layers [see Fig. 1(a)]. This misalignment inextricably links Rashba (arising from the out-of-plane dipole) and Ising (from the in-plane dipole) SOC [22,23]. Further, the large M of monolayer WTe_2 severely suppresses the ordinary orbital response that arises from H_R alone (i.e., independent of δ_z) that is typically found in small M systems such as HgTe quantum wells [5,12,13]. Indeed, COM [Fig. 2(a)] is consistent with the sizable out-of-plane edge gap opening recently measured in WTe_2 monolayers [18,20].

To obtain the full edge magnetoresponse, we also include the (pure spin) Zeeman effect where magnetic field directly couples with $\mathbf{s}$ in the bulk. These only contribute to the diagonal terms of g_{ij} in Eq. (1), and do not induce a gap opening along the edge when $\mathbf{B} = B_z\hat{\mathbf{z}}$ [12–14] (see SM for a discussion [24]). Taking typical values of bulk Lande g-factors ≈ 2 and projecting onto the edge, we obtain $g_{xx}, g_{yy} \sim 1.2$–2.0 which weakly depend on δ_x, δ_z (see SM [24]). Combining orbital (off-diagonal) and spin Zeeman (diagonal) terms in Eq. (1), we obtain an anisotropic B-field-induced edge full gap $\Delta(\mathbf{B})$ [Figs. 1(b) and 1(c)].

Crucially, for most orientations of $\mathbf{B}$ (when azimuthal $\varphi \neq 90^\circ$), we find that $\Delta(\mathbf{B})$ is minimized at an oblique polar angle, i.e., θ is neither zero nor 90°. This is in stark contrast to that found in HgTe QSH systems where the minimal gap occurs when $\theta = 90^\circ$ [5]. Strikingly, when $\mathbf{B}$ lies in the x-z plane (azimuthal $\varphi = 0$), $\Delta(\mathbf{B})$ nearly vanishes at a critical angle θ_c

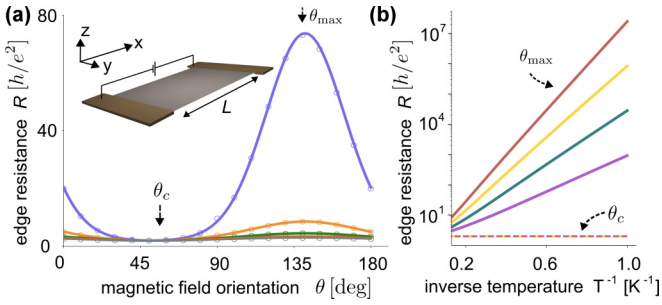

FIG. 3. Edge magnetoresistance $R(\mathbf{B})$ for the magnetic field directed in the x-z plane, i.e., $\mathbf{B} = |\mathbf{B}|(\sin\theta, 0, \cos\theta)$. (a) $R(\mathbf{B})$ varies with θ at different temperatures $T = 2, 4, 6, 8, 10$ K (top to bottom) and at a fixed $|\mathbf{B}| = 7$ T. $R(\mathbf{B})$ displays no temperature variation at θ_c; in contrast, $R(\mathbf{B})$ exhibits large temperature changes at $\theta_{\max}$. Solid lines are obtained using the edge Hamiltonian in Eq. (1), and circles are obtained from the edge spectrum ENS displaying good agreement. (b) $R(\mathbf{B})$ taken at $\theta_{\max}$ (solid curves) display thermally activated behavior with the slope increasing as $|\mathbf{B}| = 6, 8, 10, 12$ T increases (bottom to top). In contrast, $R(\mathbf{B})$ at θ_c (dashed lines) does not change with temperature or with magnetic field. See SM [24] for detailed transport parameters. The other parameters used are the same as in Fig. 1.

[see the blue curve in Fig. 1(b)]; indeed, the residual gap θ_c is 3.5 μeV (obtained from Fig. 2)—two orders of magnitude smaller than the maximum gap opening [Fig. 1(b)]. Noting that $g_{xz} \gg g_{yz}$ and specializing to $\mathbf{B} = |\mathbf{B}|(\sin\theta, 0, \cos\theta)$ in the x-z plane, we find

$$\Delta(\mathbf{B}) \approx g_{\text{eff}}\mu_B|\mathbf{B}||\sin(\theta - \theta_c)|, \quad \tan\theta_c = -\frac{g_{xz}}{g_{xx}}, \qquad (9)$$

where $g_{\text{eff}} = \sqrt{g_{xx}^2 + g_{xz}^2}$. Taking $\delta_z = 70$ meV and $\delta_x = 40$ meV as an illustration, we obtain $\theta_c = 51^\circ$ [Fig. 1(b)]. $\Delta(\mathbf{B})$ exhibits a 180° periodicity; the next zero in Eq. (9) occurs at $\theta = \theta_c + 180^\circ$. Maximal $\Delta(\mathbf{B})$ occurs when $\theta = \theta_{\max} = \theta_c + 90^\circ$. We note that when $\mathbf{B}$ is directed in planes other than x-z, such near vanishing of the gap does not occur [see, e.g., Fig. 1(c), green and red curves], and is nonvanishing and sizable in all directions.

While we have concentrated on edges along the x direction, we note that edge termination as well as orientation can also influence the edge behavior in WTe_2 [28,29]. Nevertheless, we expect that COM can persist for other edge orientations [see, e.g., SM [24] for an illustration of $\Delta(\mathbf{B})$ and COM for other edge orientations].

In Fig. 3(a) we plot the edge magnetoresistance $R(\mathbf{B})$ for an edge along the x direction for a fixed magnitude of magnetic field $|\mathbf{B}| = 7$ T but applied at various orientations of $\mathbf{B}$ along the x-z plane (i.e., $\varphi = 0$), namely $\mathbf{B} = |\mathbf{B}|(\sin\theta, 0, \cos\theta)$ (see SM [24], and also Refs. [30–33] therein, for a detailed description). Edge magnetoresistance is large and highly sensitive to a temperature close to $\theta = \theta_{\max}$ where the edge gap is largest; as the temperature is lowered, the magnetoresistance climbs rapidly in an exponential fashion [Fig. 3(b)].

In contrast, close to $\theta = \theta_c$ the edge magnetoresistance remains nearly constant with temperature since the gap opening close to θ_c almost vanishes [see the blue curves in Figs. 1(b) and 1(c)]. Indeed, the curves at various temperatures in Figs. 3(a) and 3(b) collapse on each other at $\theta = \theta_c$. The insensitivity of magnetoresistance to temperature provides a direct experimental means to determine $\hat{\mathbf{B}}_*$—the direction wherein the applied magnetic field is ineffective at gapping out the edge states. Away from the x-z plane, i.e., $\varphi \neq 0$, we note that resistance curves at various temperatures no longer collapse on each other for any value of θ since $\Delta(\mathbf{B})$ is generically finite and sizable in all directions when $\varphi \neq 0$.

COM is a direct consequence of the cooperation between $\mathcal{H}_R$ and $\mathcal{H}_I$ that plays a critical role in both the edge spin structure and its magnetoresponse. Given the tight spatial confinement of the edge wave functions $\sim 2C_y/v_y = 1.9$ nm for typical WTe_2 parameters, we expect that the edge magnetoresponse is most sensitive to $\mathcal{H}_{R,I}$ in the region close to the edge, where, for example, strong confining edge electric fields will inevitably appear close to the sample boundaries [34]. Additionally, while here we have concentrated on COM and its relation to $\mathcal{H}_R$ and $\mathcal{H}_I$, we remark that the cooperative spin canting mechanism is general and can also ensue with other SOC mechanisms. Perhaps most striking, from a technological perspective, is the near zero in magnetoresistance that enables very large AMR: Comparing resistance at 10 T for $\theta_{\max}$ and θ_c [Fig. 3(b)] we expect giant AMR as large as several million percent at low temperature can be achieved in WTe_2 competitive with other large magnetoresistance materials at similar $\mathbf{B}$ and temperature ranges [35,36].

We thank David Cobden, Wenjin Zhao, and Valla Fatemi for useful conversations. This work was supported by the National Research Foundation (NRF) Singapore under NRF Fellowship Award No. NRF-NRFF2016-05, a Nanyang Technological University start-up grant (NTU-SUG), and a Ministry of Education Singapore Academic Research Fund Tier 3 Grant No. MOE2018-T3-1-002.

[1] C. L. Kane and E. J. Mele, Phys. Rev. Lett. **95**, 146802 (2005).
[2] B. A. Bernevig, T. L. Hughes, and S. C. Zhang, Science **314**, 1757 (2006).
[3] C. Wu, B. A. Bernevig, and S. C. Zhang, Phys. Rev. Lett. **96**, 106401 (2006).
[4] M. König, S. Wiedmann, C. Brüne, A. Roth, H. Buhmann, L. W. Molenkamp, X. L. Qi, and S. C. Zhang, Science **318**, 766 (2007).
[5] M. König, H. Buhmann, L. W. Molenkamp, T. L. Hughes, C. X. Liu, X. L. Qi, and S. C. Zhang, J. Phys. Soc. Jpn. **77**, 031007 (2008).
[6] B. Zhou, H.-Z. Lu, R.-L. Chu, S.-Q. Shen, and Q. Niu, Phys. Rev. Lett. **101**, 246807 (2008).
[7] M. Bütiker, Science **325**, 278 (2009).
[8] M. Z. Hasan and C.L. Kane, Rev. Mod. Phys. **82**, 3045 (2010).
[9] X. L. Qi and S. C. Zhang, Rev. Mod. Phys. **83**, 1057 (2011).
[10] S. Q. Shen, *Topological Insulators* (Springer, Berlin, 2012).

[11] X. Qian, J. Liu, L. Fu, and J. Li, Science **346**, 1344 (2014).
[12] J. Maciejko, X. L. Qi, and S. C. Zhang, Phys. Rev. B **82**, 155310 (2010).
[13] M. V. Durnev and S. A. Tarasenko, Phys. Rev. B **93**, 075434 (2016).
[14] F. Dominguez, B. Scharf, G. Li, J. Schäfer, R. Claessen, W. Hanke, R. Thomale, and E. M. Hankiewicz, Phys. Rev. B **98**, 161407(R) (2018).
[15] C. Liu, T. L. Hughes, X. L. Qi, K. Wang, and S. C. Zhang, Phys. Rev. Lett. **100**, 236601 (2008).
[16] I. Knez, R. R. Du, and G. Sullivan, Phys. Rev. Lett. **107**, 136603 (2011).
[17] T. Li, P. Wang, H. Fu, L. Du, K. A. Schreiber, X. Mu, X. Liu, G. Sullivan, G. A. Csáthy, X. Lin, and R. R. Du, Phys. Rev. Lett. **115**, 136804 (2015).
[18] Z. Fei, T. Palomaki, S. Wu, W. Zhao, X. Cai, B. Sun, P. Nguyen, J. Finney, X. Xu, and D. H. Cobden, Nat. Phys. **13**, 677 (2017).
[19] S. Tang, C. Zhang, D. Wong, Z. Pedramrazi, H. Z. Tsai, C. Jia, B. Moritz, M. Claassen, H. Ryu, S. Kahn, J. Jiang, H. Yan, M. Hashimoto, D. Lu, R. G. Moore, C. C. Hwang, C. Hwang, Z. Hussain, Y. Chen, M. M. Ugeda *et al.*, Nat. Phys. **13**, 683 (2017).
[20] S. Wu, V. Fatemi, Q. D. Gibson, K. Watanabe, T. Taniguchi, R. J. Cava, and P. Jarillo-Herrero, Science **359**, 76 (2018).
[21] Y. Shi, J. Kahn, B. Niu, Z. Fei, B. Sun, X. Cai, B. A. Francisco, D. Wu, Z. X. Shen, X. Xu, D. H. Cobden, and Y. T. Cui, Sci. Adv. **5**, eaat8799 (2019).
[22] S. Y. Xu, Q. Ma, H. Shen, V. Fatemi, S. Wu, T. R. Chang, G. Chang, A. M. M. Valdivia, C. K. Chan, Q. D. Gibson, J. Zhou, Z. Liu, K. Watanabe, T. Taniguchi, H. Lin, R. J. Cava, L. Fu, N. Gedik, and P. Jarillo-Herrero, Nat. Phys. **14**, 900 (2018).
[23] L. K. Shi and J. C. W. Song, Phys. Rev. B **99**, 035403 (2019).
[24] See Supplemental Material at http://link.aps.org/supplemental/10.1103/PhysRevB.102.161402 for a discussion of symmetry in WTe_2 as well as parameter values, exact numerical solution of edge states as well as a zero mode analysis, analytical derivation of the orbital magnetoresponse, spin Zeeman magnetoresponse, edge states along other edge orientations, as well as numerical edge resistance at various angles and temperatures, which includes Refs. [25,30–33].
[25] R. Winkler, *Spin-Orbit Coupling Effects in Two-Dimensional Electron and Hole Systems* (Springer, Berlin, 2003).
[26] D. G. Rothe, R. W. Reinthaler, C. X. Liu, L. W. Molenkamp, S. C. Zhang, and E. M. Hankiewicz, New J. Phys. **12**, 065012 (2010).
[27] W. Beugeling, N. Goldman, and C. M. Smith, Phys. Rev. B **86**, 075118 (2012).
[28] A. Lau, R. Ray, D. Varjas, and A. R. Akhmerov, Phys. Rev. Materials **3**, 054206 (2019).
[29] S. Ok, L. Muechler, D. Di Sante, G. Sangiovanni, R. Thomale, and T. Neupert, Phys. Rev. B **99**, 121105(R) (2019).
[30] N. W. Ashcroft and N. D. Mermin, *Introduction to Solid State Physics* (Brooks Cole, New York, 1976).
[31] M. Lundstrom, *Fundamentals of Carrier Transport* (Cambridge University Press, Cambridge, UK, 2009).
[32] G. Giuliani and G. Vignale, *Quantum Theory of the Electron Liquid* (Cambridge University Press, Cambridge, UK, 2005).
[33] A. C. Balram, K. Flensberg, J. Paaske, and M. S. Rudner, Phys. Rev. Lett. **123**, 246803 (2019).
[34] D. B. Chklovskii, B. I. Shklovskii, and L. I. Glazman, Phys. Rev. B **46**, 4026 (1992).
[35] T. Liang, Q. Gibson, M. N. Ali, M. Liu, R. J. Cava, and N. P. Ong, Nat. Mater. **14**, 280 (2015).
[36] M. N. Ali, J. Xiong, S. Flynn, J. Tao, Q. D. Gibson, L. M. Schoop, T. Liang, N. Haldolaarachchige, M. Hirschberger, N. P. Ong, and R. J. Cava, Nature (London) **514**, 205 (2014).